

# Superconductor strip with transport current: Magneto-optical study of current distribution and its relaxation

A. V. Bobyl<sup>1,2</sup>, D. V. Shantsev<sup>1,2</sup>, Y. M. Galperin<sup>1,2</sup>, T. H. Johansen<sup>1,\*</sup>, M. Baziljevich<sup>1</sup>, and S. F. Karmanenko<sup>3</sup>

<sup>1</sup>*Department of Physics, University of Oslo, P. O. Box 1048 Blindern, 0316 Oslo, Norway*

<sup>2</sup>*A. F. Ioffe Physico-Technical Institute, Polytekhnicheskaya 26, St. Petersburg 194021, Russia*

<sup>3</sup>*Electrotechnical University, Prof. Popov Str. 5, St. Petersburg, 197376, Russia*

The dynamics of magnetic flux distributions across a  $\text{YBa}_2\text{Cu}_3\text{O}_{7-\delta}$  strip carrying transport current is measured using magneto-optical imaging at 20 K. The current is applied in pulses of 40-5000 ms duration and magnitude close to the critical one, 5.5 A. During the pulse some extra flux usually penetrates the strip, so the local field increases in magnitude. When the strip is initially penetrated by flux, the local field either increases or decreases depending both on the spatial coordinate and the current magnitude. Meanwhile, the current density always tends to redistribute more uniformly. Despite the relaxation, all distributions remain qualitatively similar to the Bean model predictions.

## I. INTRODUCTION

In many technological applications like high- $T_c$  bolometers and electrical power cables the superconductors are subjected to pulses of transport current. If the current is small, the magnetic flux behavior in superconductors with strong bulk pinning is described by the critical-state model (CSM).<sup>1</sup> According to the model, the magnetic flux is frozen, and the current density  $j$  is everywhere equal to (or less than) its critical value,  $j_c$ . Flux and current distributions in superconductors carrying a transport current were measured in several previous works. Among them are results obtained using magneto-optical (MO) imaging,<sup>2-9</sup> Hall micro-probes,<sup>10-12</sup> and detection based on THz radiation.<sup>13</sup>

If the transport current  $I$  exceeds its critical value  $I_c$  the CSM description becomes invalid. In this case the flux starts to move through the superconductor resulting in a non-zero electric field across the sample, i. e., in a finite resistance. In reality, the transition from frozen to moving flux lattice is rather smooth, since for any value of  $I$  some regions of the superconductor carry the current density  $j \approx j_c$ . For  $I \lesssim I_c$  these regions occupy a substantial fraction of the sample, and the magnetic flux distribution becomes highly non-stationary. This is known to result in a number of dynamic effects such as voltage dependence on the current sweep rate, and resistance relaxation.<sup>14-17</sup> Direct spatially-resolved measurements of the non-stationary flux distribution could be very useful for analysis of these effects. Such measurements have already proved quite efficient for the applied field case, namely, to access the spectral distribution of the activation energies in  $\text{YBa}_2\text{Cu}_3\text{O}_{7-\delta}$  films,<sup>18</sup> and to detect transinet vortex phases in Bi-2212 crystals.<sup>19</sup> In the present paper we use the MO imaging technique to study the dynamics of flux and current distributions induced by a pulsed transport current  $I$  up to  $I_c$ . The experiments are performed on a thin strip of  $\text{YBa}_2\text{Cu}_3\text{O}_{7-\delta}$  and cover the time interval 40-5000 ms after onset of the pulse.

It turns out that the most convenient regime to study

the dynamic effects is when the strip is subjected to both a transport current and an externally applied field. Then one can create states where the CSM predicts<sup>20</sup> a region with  $j = j_c$  covering more than a half of the strip width, and therefore the deviations from the CSM are more easily detected. Such a situation has so far been studied only in a few works,<sup>4,7,12</sup> and without a systematic comparison to the CSM and with no attention to dynamic effects. Therefore, we have chosen the following two magnetic states for the present study: (i) a flux-free strip subjected to a transport current – the reference case, and (ii) a strip in the remanent state after a large field pulse plus a transport current.

The paper is organized as follows. The experimental method including the field-to-current inversion scheme is described in Sec. II. Section III presents comparison of the current density distributions for different  $I$  to the CSM predictions. The relaxation of the flux and current distributions at fixed  $I$  is analysed in Sec. IV.

## II. EXPERIMENTAL PROCEDURE

Films of  $\text{YBa}_2\text{Cu}_3\text{O}_{7-\delta}$  (YBCO) were grown by dc magnetron sputtering<sup>21</sup> on  $\text{LaAlO}_3$  substrate. X-ray and Raman spectroscopy analysis confirmed that the films were  $c$ -axis oriented and of a high structural perfection. A microbridge with dimensions  $500 \times 100 \times 0.2 \mu\text{m}^3$  was formed from the film by a standard lithography procedure. Several Au wires of  $50 \mu\text{m}$  diameter were attached to each Au/Ag contact pad using thermocompression.

The imaging system is based on the Faraday rotation of polarized light illuminating an MO-active indicator film that we mount directly on top of the superconductor's surface. The rotated Faraday angle varies locally with the value of the perpendicular magnetic field, and through an analyzer in an optical microscope one can directly visualize and quantify the field distribution across the covered sample area. As a Faraday-active indicator we use a Bi-doped ferrite garnet film with in-plane magnetization.<sup>22</sup> The indicator film was deposited to a

thickness of  $5 \mu\text{m}$  by liquid phase epitaxy on a gadolinium gallium garnet substrate. A thin layer of aluminum is evaporated onto the film allowing incident light to be reflected, thus providing double Faraday rotation of the light beam. The images were recorded with an 8-bit Kodak DCS 420 CCD camera and transferred to a computer for processing. The MO imaging at low temperatures was performed by mounting the superconductor/MO-indicator on the cold finger of a continuous He-flow cryostat with an optical window (Microstat, Oxford).

The flux distribution in a sample biased with large transport current is subjected to fast relaxation. Therefore, it was important to minimize the camera exposure time. On the other hand, very short exposures lead to poor-quality MO images, and as a compromise, 33 ms exposure time was chosen. The sample was biased with current pulses of 40 ms duration, which were synchronized with the camera recording. One image was taken during the pulse, and another image after the current was switched off. Experiments were also performed to study the relaxation of flux distributions during current pulses. For this purpose we used pulse durations up to 5000 ms. The MO images were then recorded at different times during the pulse.

As the bridge thickness is much less than its width, the theoretical results for the thin strip geometry<sup>20,23</sup> can be used. In our experiments, the bridge thickness is also of the order of the London penetration depth, hence its magnetic properties are fully characterized by the two-dimensional flux distribution at the surface.

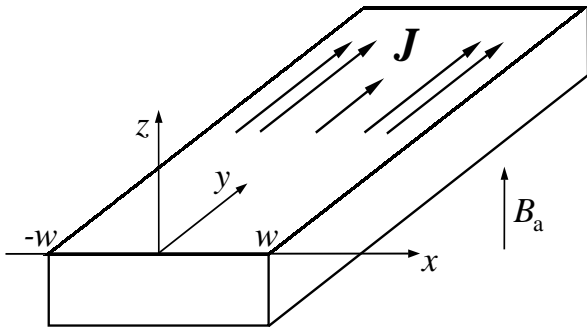


FIG. 1. Superconducting strip with transport current

The current density distribution in the strip cross section was calculated from the measured flux density distribution using the 1D inversion scheme proposed in Ref. 24. Consider a long thin superconducting strip with edges located at  $x = \pm w$ , the  $y$ -axis pointing along the strip, and the  $z$ -axis normal to the strip plane, see Fig. 1. The transport current flows in  $y$ -direction as does the screening current due to the magnetic field,  $B_a$ , applied along the  $z$ -axis. The perpendicular magnetic field at the height  $h$  above a superconductor strip, i. e. at  $-w \leq x \leq w$ , is related to the current density distribution by the Biot-Savart's law

$$B(x) = B_a + \frac{\mu_0}{2\pi} \int_{-w}^w dx' \frac{x' - x}{h^2 + (x' - x)^2} J(x'). \quad (1)$$

Here  $J(x) = \int j(x, z) dz$  is the sheet current,  $j(x, z)$  is the current density, and the integral is calculated over the strip thickness  $Z$ , where  $Z \ll w$ . Inversion of Eq. (1) yields<sup>24</sup>

$$J(n) = \sum_{n'} \frac{n - n'}{\mu_0 \pi} \left( \frac{1 - (-1)^{n-n'} e^{\pi d}}{d^2 + (n - n')^2} + \frac{[d^2 + (n - n')^2 - 1] [1 - (-1)^{n-n'} e^{\pi d}]}{[d^2 + (n - n' + 1)^2] [d^2 + (n - n' - 1)^2]} \right) B(n'). \quad (2)$$

This expression is written for discrete coordinates  $x = n\Delta$  with integer  $n$ , the ratio  $h/\Delta$  is denoted as  $d$ . The current distributions  $J(x)$  calculated from this expression are already reasonably good, see, e. g., Refs. 24,8. However, since the high- $k$  components are suppressed by the inversion procedure, the accuracy of the calculated  $J(x)$  turns out to be poor near the sample edge where the current drops abruptly to zero.

In the present work we develop an improved inversion scheme using an iteration procedure. Suppose we know  $J_N(x)$  calculated on the  $N$ th iteration step. We then set  $J_N(x)$  equal to zero outside the superconductor, and substitute the new current distribution into Eq. (1) to get the flux distribution  $B_N(x)$ . The latter will be slightly different from the measured distribution  $B(x)$ . The difference  $B(x) - B_N(x)$  is then substituted into Eq. (2) to calculate  $\delta J_N(x)$ . We then set  $J_{N+1}(x) = J_N(x) + \delta J_N(x)$  and start the next iteration. After each iteration step  $B_N(x)$  approaches closer to  $B(x)$ , and the current near the edge drops more abruptly. It is usually sufficient to perform 5-10 iterations. The final current distribution exhibits an abrupt jump at the sample edges as can be seen from the figures below and a test example discussed in Appendix A. In the calculations we also took into account effect of the component  $B_x$  on the MO indicator sensitivity.<sup>24</sup>

### III. PULSES WITH DIFFERENT MAGNITUDE

#### A. Transport current

The MO images for an initially flux-free strip carrying a transport current were taken at 20 K. The image for the highest current,  $I = 4.9$  A, is shown in Fig. 2. The image was taken with slightly uncrossed polarizer and analyzer. This provides that the flux density of different polarity shows up as different gray level. Consequently, the MO images can be directly converted into a flux density distribution using a careful calibration curve. The flux distributions were calculated for the area marked by the black rectangle in Fig. 2 and then averaged along the strip.

Six profiles of the flux density  $B(x)$  across the strip for different currents are shown in Fig. 3(a). The flux density has opposite signs at the left and the right parts of the strip, and  $|B|$  is maximal near the edges. The corresponding current density profiles, Fig. 3(b), are calculated by the inversion scheme, using  $h = 12\mu\text{m}$ . The experimental current profiles reproduce well the main features of the Bean-model result, Fig. 3(c), where the current density is always minimal at the center of the strip. On the other hand, the model predicts constant  $J(x) = J_c$  near the edges. Instead, experimentally we find maxima in  $J(x)$  their magnitude and position being dependent on  $I$ . This behavior is in agreement with flux creep simulations,<sup>25,8</sup> hence these deviations from the CSM can be related to dynamic effects.

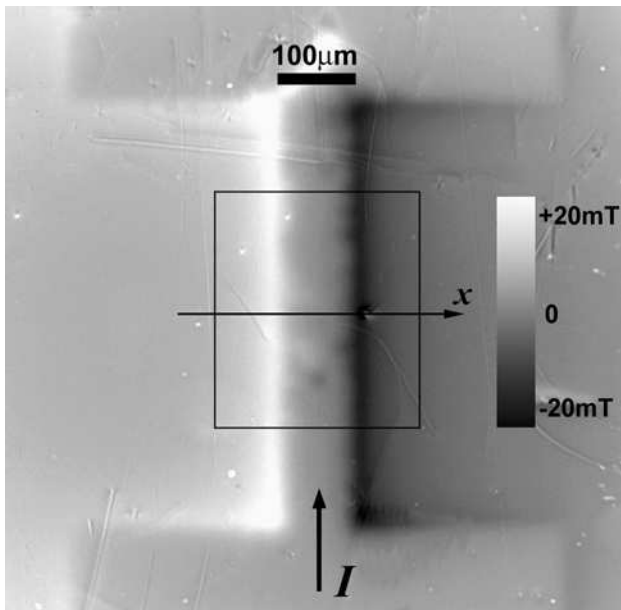


FIG. 2. MO image of YBCO strip carrying transport current 4.9 A. The image is obtained with uncrossed polarizers so that the positive and negative flux density correspond to bright and dark regions, respectively. The black rectangle shows the image area used for calculation of the current density distribution.

When the transport current  $I$  is switched off, the magnetic flux in the inner part of the strip remains trapped. The return field of this trapped flux re-magnetizes the edge regions of the strip and flux of opposite sign penetrates an outer rim. Flux density profiles for such a remanent state taken across the strip are shown in Fig. 4(a). The central part of these profiles is similar to that of the corresponding profiles in the current-carrying state, Fig. 3(a). However, typical values of  $|B|$  are much smaller, in agreement with the Bean model, therefore the scale of  $y$ -axis is different.

The current density profiles are shown in Fig. 4(b) along with the Bean-model profiles, panel (c). As the net current must be zero in any cross section, current

lines should form closed loops. In the center, the current keeps flowing in the same direction as the transport current, while near the edges it now flows backwards. This result is nicely reproduced in our experiment. Moreover, in agreement with the Bean model we find that (i) the current density is maximal near the edges, (ii) the boundary between positive and negative  $J$  shifts inwards as  $I$  increases. Nevertheless, like in the current-carrying state, we don't find an agreement with the theory near the edges where  $J(x)$  should be always equal to  $J_c$ .

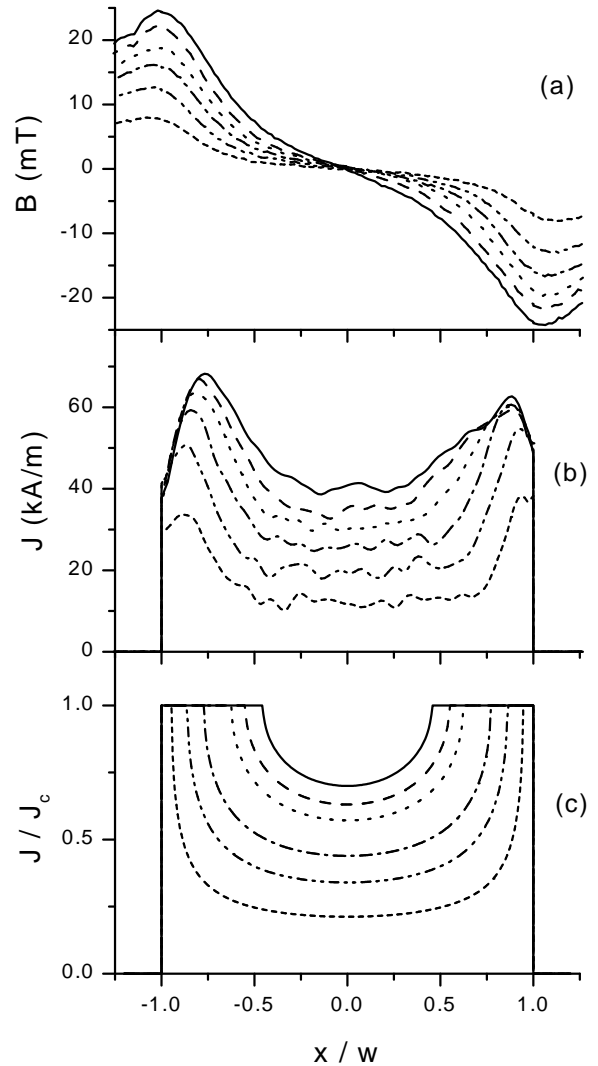


FIG. 3. Initially flux-free YBCO strip carrying transport current  $I=1.8, 2.8, 3.5, 4.3, 4.6,$  and  $4.9$  A. (a,b) experimental flux and current density profiles determined from MO images like in Fig. 2, (c) the CSM current density profiles, Eq. (1), with  $I_c = 5.5$  A. The flux density data were obtained from MO images of the strip, and the plot  $B(x)$  is the average profile in a  $300\mu\text{m}$  wide band across the strip.

The flux dynamics is expected to proceed much faster in the regions where the current density is close to the

critical one. It is exactly those edge regions where the deviations from the Bean behavior are found. However, in the above experiment, the size of these regions was relatively small,  $0.6 - 0.9w < |x| < w$ . Thus, the results could possibly be affected by inaccuracy of the inversion method or small defects near the strip edge. For this reason we performed another experiment where the region of  $j \approx j_c$  is much more extended, and unambiguous manifestations of the dynamic effects are found.

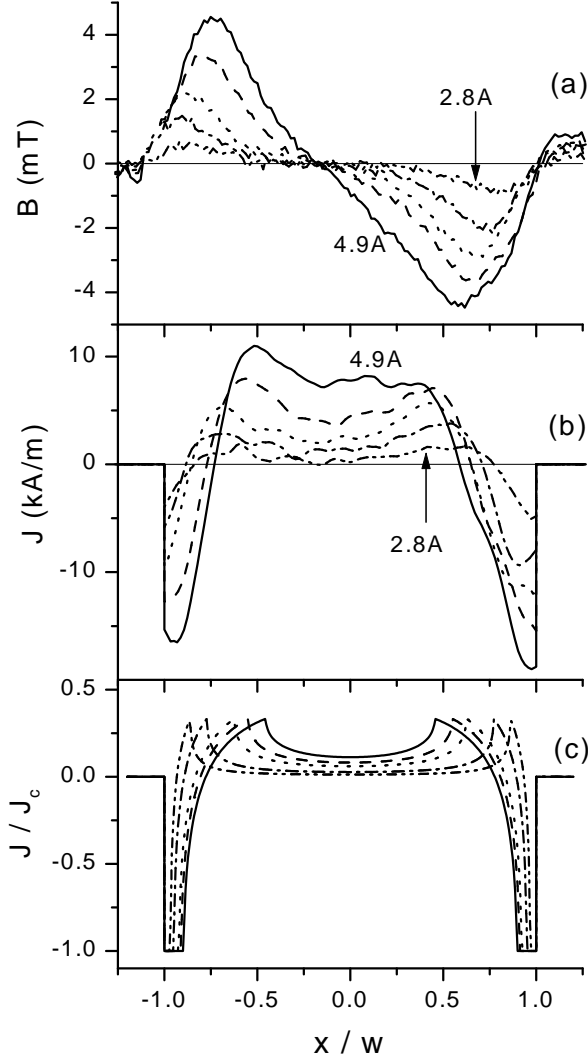


FIG. 4. Remanent state of initially flux-free YBCO strip after a current pulse with  $I=2.8, 3.5, 4.3, 4.6,$  and  $4.9$  A. (a,b) experimental flux and current density profiles, (c) the CSM current density profiles, Eq. (2) with  $I_c = 5.5$  A.

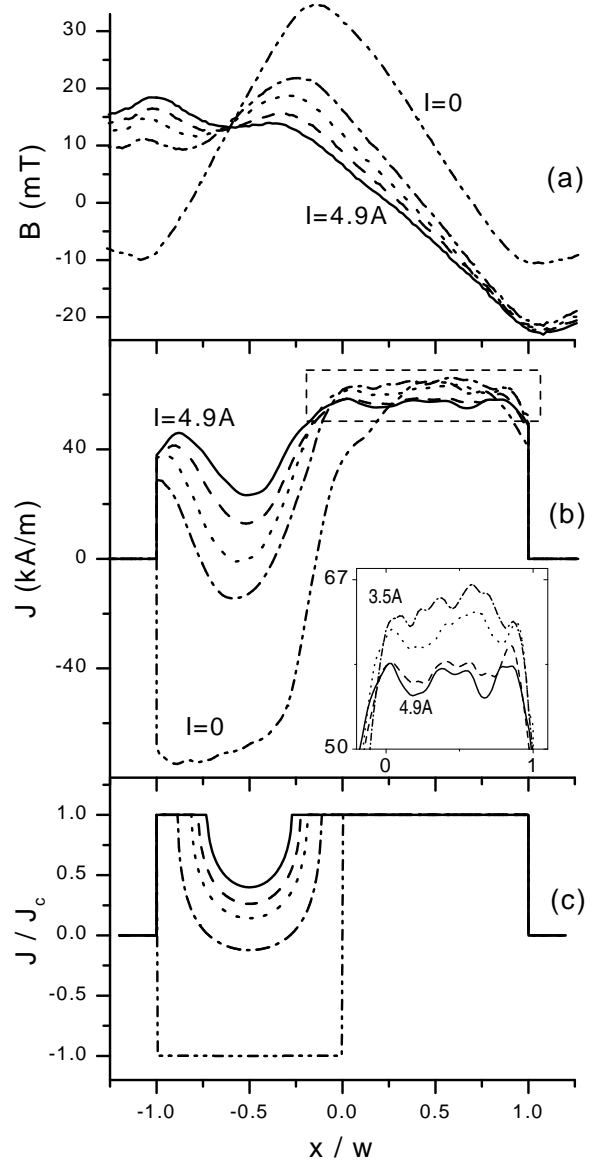


FIG. 5. YBCO strip, initially in fully-penetrated state, carrying transport current  $I=0, 3.5, 4.3, 4.6,$  and  $4.9$  A. (a,b) experimental flux and current density profiles, (c) the CSM current density profiles, Eq. (3), with  $I_c = 5.5$  A. Inset in (b) is a blow-up of the dashed rectangle.

## B. Remanent Field + Transport current

In the second experiment, a large magnetic field was applied to the strip and subsequently removed. As a result, some flux remain trapped in the strip, and the flux profile has a conventional triangular shape with maximum at the center, see the “ $I = 0$ ” curve in Fig. 5(a). Small regions near the edges,  $|x| > w/\sqrt{2}$  are filled with return field of the opposite polarity. The strip was then biased with transport current  $I$ , and flux density dis-

tributions were measured in the current-carrying state.  $B(x)$  profiles across the strip for different  $I$  are shown in Fig. 5(a). As the current increases, the central peak diminishes, and almost disappears at the maximal current (solid line). Meanwhile, another peak at the left edge shows up and grows with  $I$ . At intermediate currents one can clearly see two peaks in  $B(x)$  profile. This feature was predicted long ago within the Bean model analysis,<sup>20</sup> but has not so far been observed in experiment.

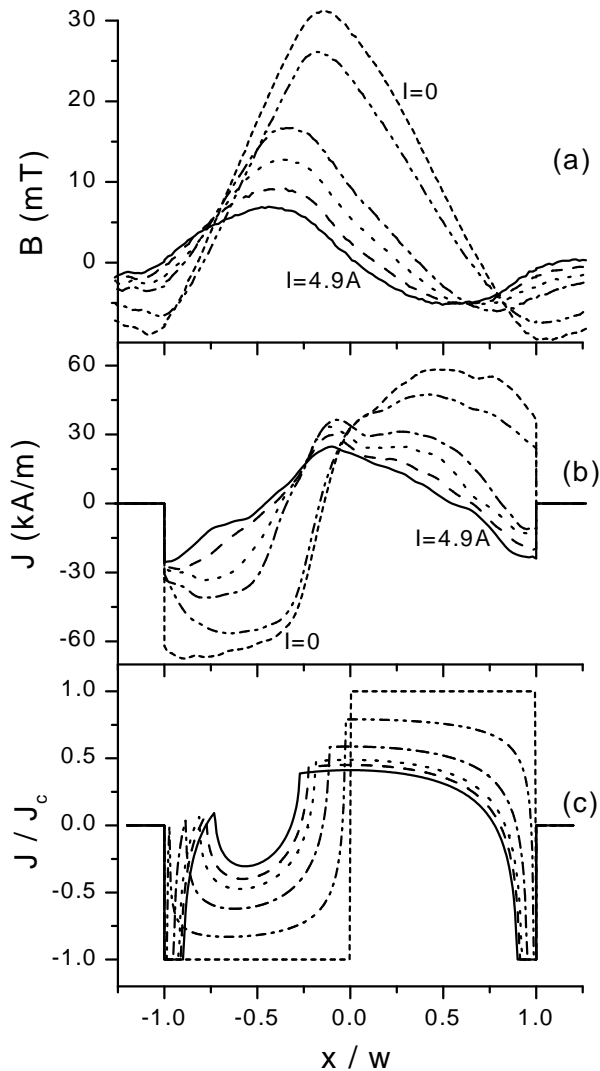


FIG. 6. Remanent state of initially fully-penetrated YBCO strip after a current pulse  $I=0, 1.8, 3.5, 4.3, 4.6,$  and  $4.9$  A. (a,b) experimental flux and current density profiles, (c) the CSM current density profiles, Eq. (4), with  $I_c = 5.5$  A.

The current density profiles are presented in Fig. 5(b) along with the Bean model profiles, panel (c). According to the model, the current distribution in the left half is actually a copy of the distribution for the “pure” transport current state, Fig. 3(c), though squeezed in  $x$ -direction.

Thus,  $J(x)$  profile has a deep minimum at the middle of the left half, which is well reproduced in the experimental profiles. However, we find a clear disagreement with the theory in the right half of the strip. There the Bean model predicts a flat  $J(x)$  unaffected by the transport current. In experiment,  $J(x)$ , though being quite flat appears dependent on  $I$ . This is emphasized in the inset, where one can see a monotonous *decrease* of  $J(x)$  level as the current *increases*. Such a behavior contradicts not only the Bean model but also common intuition. This interesting observation is discussed below in the framework of relaxation effects.

The remanent flux and current distributions after the current pulse are shown in Fig. 6. One can clearly see a current-induced suppression and shift of the peak in  $B(x)$ , as predicted by the Bean model,<sup>20</sup> and observed earlier.<sup>12</sup> However, the current density profile is too complicated to make any solid conclusions. We mention only two main features of the Bean profiles found also experimentally: (i) a peak in  $J(x)$  at small negative  $x$ , (ii) a concave shape of the profile in the left, and convex in right half of the strip.

#### IV. RELAXATION DURING THE PULSE

In order to understand the reason for the observed deviations of the measured  $B$ - and  $J$ -profiles from the CSM predictions we analyze the effect of pulse duration. It was found that the flux distribution does not remain fixed during the current pulse, even though the current magnitude is kept constant. The flux is subjected to relaxation which is especially fast for larger currents.

The relaxation effects are known to be noticeable in high-temperature superconductors even in the absence of transport current due to large flux creep rates.<sup>26</sup> The direction in which the relaxation proceeds can be always well understood. In a conventional experiment, the flux trapped in a superconductor kept at zero applied field monotonously decreases with time. This means that the flux density decreases in amplitude throughout the sample. If a sample is kept in constant non-zero applied field  $H_a$ , then the flux distribution relaxes towards a uniform  $H(\vec{r}) = H_a$ . Remarkably, for a thin sample in a perpendicular field there coexist regions with  $H > H_a$ , where  $H$  decreases due to creep, and regions with  $H < H_a$ , where  $H$  increases.<sup>27,28</sup> They are separated by a so-called neutral line, where the flux density remains constant.

In the presence of transport current the relaxation of flux and current density profiles is even more complicated as illustrated by Figs. 7, and 8. Flux distributions were measured at different times during the pulse starting from  $t = 40$  ms up to 5000 ms ( $t = 0$  corresponds to switching current on). Fig. 7 shows the results for the case of initially flux-free strip with  $I = 4.9$  A, like in Fig. 3. Only the first ( $t = 40$  ms) and the last ( $t = 1600$  ms)  $B(x)$  profiles are presented. The two cor-

responding  $J(x)$  profiles are indicated by thick solid and thick dashed line respectively at the bottom panel.

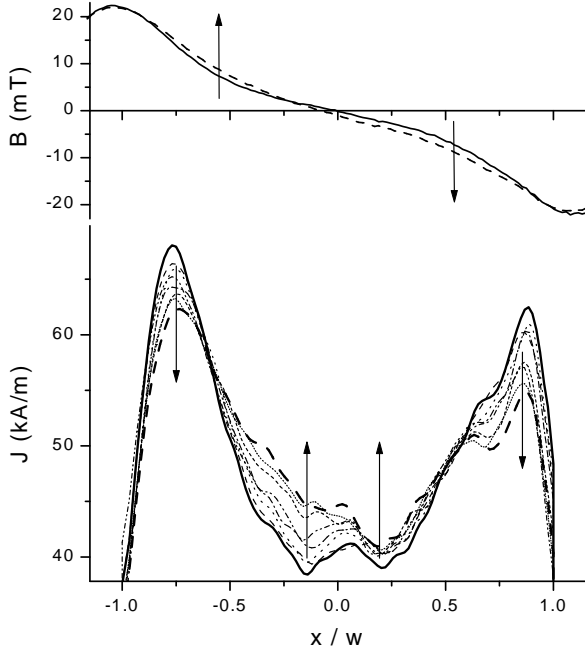


FIG. 7. Relaxation of flux and current density distribution in an initially flux-free YBCO strip during the current pulse,  $I = 4.9$  A. The profiles correspond to different times: 40, 100, 200, 300, 450, 800, 1200, and 1600 ms; arrows show the time direction. The absolute flux density increases throughout the sample. The current tends to redistribute more uniformly: some extra current moves from the edges to the central region.

We note that, in contrast to the applied field case, the relaxation leads to *increasing* the field amplitude throughout the superconductor. This means that more and more flux enters the sample as the time passes. In terms of  $J$ -profile it means that some extra current redistributes from the edges to the center. It can be also interpreted as a tendency for  $J$ -distribution to become more uniform.

Shown in Fig. 8 are results for the combined “remanent field + transport current” state, with  $I = 3.5$  and  $4.9$  A. Here the relaxation of  $B(x)$  does not follow a simple rule. The flux density may increase or decrease depending on the position in the sample, and on the current amplitude. Moreover, a closer look shows that the direction of relaxation may change as the relaxation proceeds, like in Fig. 8(a) at  $x \approx -0.8w$ . However, the changes in  $J$ -profile have the same tendency as for the flux-free strip subjected to transport current: the current tends to distribute more uniformly.

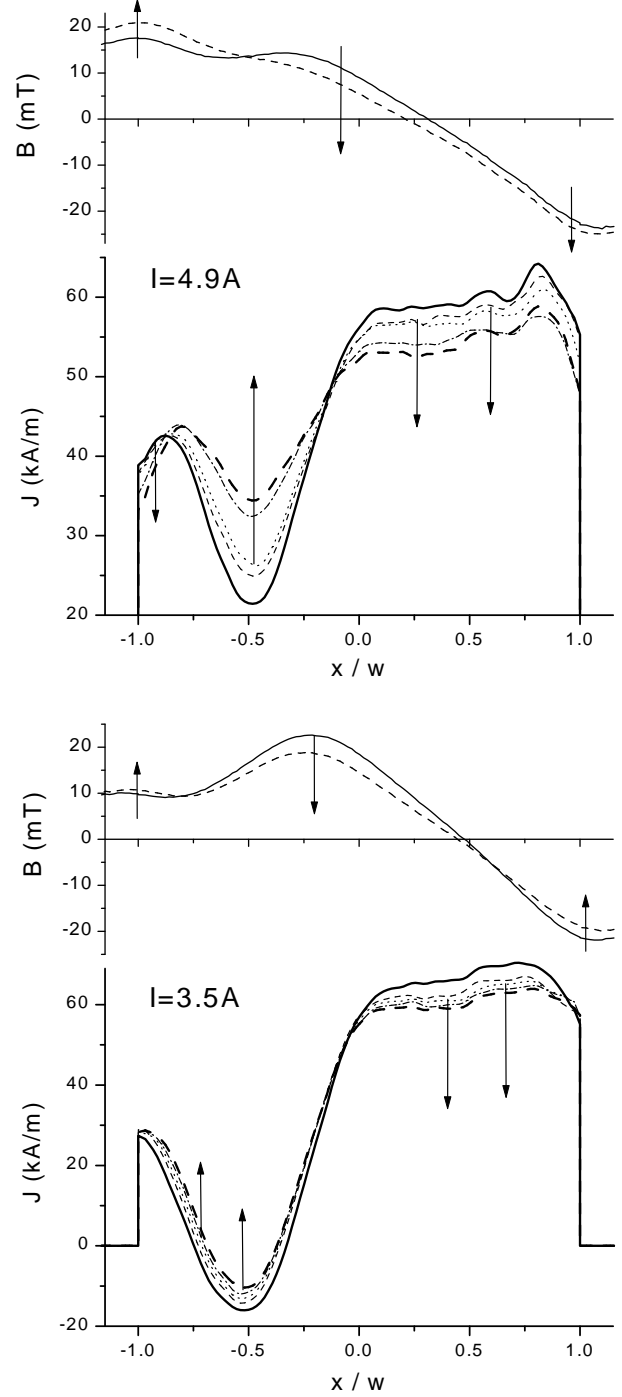


FIG. 8. Relaxation of flux and current density distribution during the current pulse for the “remanent field + current” state. Top:  $I = 4.9$  A, times: 40, 100, 200, 800 and 1600 ms. Bottom:  $I = 3.5$  A, times: 40, 400, 800, 1600, and 5000 ms. Arrows show the time direction. The current tends to redistribute more uniformly: some extra current moves from the high-current right half to the low-current left half.

In Refs. 29,30, the relaxation of the local flux density measured by a Hall sensor was described using an “effective” CSM with a *time-dependent* critical current

density. This description is basically in agreement with our results. Indeed, when  $J_c$  decays with time, the CSM predicts more and more uniform  $J(x)$ -distribution until at some point one comes to a completely uniform  $J(x) = J_c(t)$ . The rate of the  $J_c$  decay can be estimated from the plateau in  $J(x)$ -profiles at  $x > 0$  in Fig. 8. We find that from  $t = 40$  to 5000 ms the  $J_c$  reduction was  $\approx 10\%$ .

We have also performed computer simulations of flux creep based on the Maxwell equation, and Bio-Savart's law for a thin strip, Eq. (1), and logarithmic current dependence of the pinning energy.<sup>8,25</sup> The direction in which the relaxation of flux and current proceeds was always in agreement with our experimental results. The same tendency has been also found in simulations reported in Ref. 17.

However, the creep simulations do not explain the decrease of  $J$  with transport current increase illustrated in the inset of Fig. 5. One can see from comparison of the top and bottom panels of Fig. 8 that this apparent decrease is related to a faster relaxation of  $J$ -distribution for larger  $I$ . Consequently, the relaxation rate of  $J_c$  turns out to be  $I$ -dependent. The explanation of this effect remains an open question. One can expect that at larger currents a slow permanent flow of vortices across the strip sets in, probably along a few channels. This permanent flow does not change the global flux distribution and cannot be resolved magneto-optically. However, it keeps vortices in motion which should reduce  $J_c$  and assist relaxation processes.

## V. CONCLUSION

We have studied the dynamics of flux and current density distributions in a YBCO strip subjected to a pulse of transport current at 20 K. Relaxation of the distributions during the pulse is much different from the conventional relaxation of trapped flux in the absence of current. The local flux density may decrease or increase depending on the position in the sample, current amplitude, and magnetic history. However, the relaxation of  $J$ -distribution always has the same tendency: the current tends to redistribute more uniformly. Despite the relaxation, most flux and current distributions remain in a qualitative agreement with the Bean model predictions and can be described by a Bean model with a time-dependent  $J_c$ . However the behavior for the current-carrying strip in initially fully-penetrated state is not fully understood. This behavior is suggested to be associated with a flux-flow induced reduction of  $J_c$ .

## ACKNOWLEDGMENTS

The financial support from the Research Council of Norway, from the RFBR "Scientific Schools" project 00-

15-96812, and Russian Program for Superconductivity, project No 98031, is gratefully acknowledged. We are grateful to Bjørn Berling for a many-sided help.

## APPENDIX A: THE INVERSION METHOD

We demonstrate here advantages of the proposed iteration inversion method for calculation of the current density profile  $J(x)$  across the strip from the measured field profile. For this purpose we use a model example of a strip with Bean-model  $J(x)$  given by Eq. (1), with  $a = 0.5w$ . The corresponding flux density profile  $B(x)$  at the height  $h$  above the strip is given by Eq. (1). To model our experimental situation we assume that  $B(x)$  is measured in the range  $-4w < x < 4w$  at fixed  $x$  separated by  $\Delta = 0.02w$ , and that  $h = 0.2w$ .

First, we restore the current density profile using the standard procedure based on Eq. (2). Straightforward calculations where  $d = h/\Delta = 10$  produce highly oscillating  $J(x)$  due to contribution of higher harmonics, see 24. The best results are obtained by the choice  $d = 2$ , which means that only  $B$ -values at  $x$  separated by  $h/2$  are used. This  $J(x)$  profile shown by the dashed line in Fig. 9 reproduces qualitatively the initial  $J$ -profile (dotted line). There are, however, large distortions near the edges, and an error in the overall current magnitude.

The solid line shows the  $J$ -profile obtained by the iteration procedure described in Sec. II.C, for 5 iterations. It is clear from the figure that the iteration method is more successful in restoring the correct  $J$ -profile. It should be noted that the exact form of Eq. (2) is not essential for the iteration procedure. It can be modified if it will help improve convergence of  $B_N(x)$  towards  $B(x)$ . The best convergence is found when parameter  $d$  is equal to unity or less.

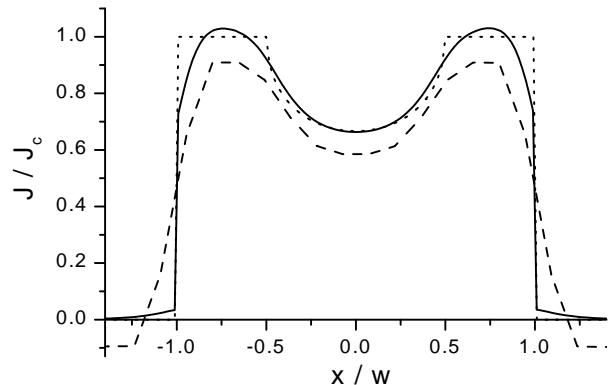


FIG. 9. Current density distributions obtained by iterative inversion procedure (solid line), and standard procedure (dashed line) for a Bean-model field distribution. The dotted line is Bean-model current distribution.

The advantage of the iteration procedure is explained by the fact that the inversion formula, Eq. (2), is used to calculate only  $\delta J_N(x)$  instead of the whole  $J(x)$ . Normally,  $\delta J_N(x)$  is much smaller and smoother than  $J_N(x)$ . Thus, an inevitable error intrinsic to any inversion procedure is minimized. The only assumption used by this procedure is that current cannot flow outside the superconductor sample, which is physically well-grounded. The location of the sample edges can be determined with

high accuracy from a simple optical image.

## APPENDIX B: BEAN-MODEL RESULTS

Here we list some Bean-model expressions for current density distributions in a thin superconducting strip obtained in Refs. 20 and 23. For an initially flux-free strip  $-w \leq x \leq w$ , Fig. 1, carrying transport current  $I$

$$\frac{J(x)}{J_c} = \begin{cases} \frac{2}{\pi} \arctan\left(\sqrt{\frac{w^2-a^2}{a^2-x^2}}\right), & |x| < a \\ 1, & a < |x| < w \end{cases}, \quad (1)$$

where  $a = w\sqrt{1-(I/I_c)^2}$ , and  $I_c = 2wJ_c$  is the critical current. This distribution is shown in Fig. 3(c). In the remanent state, after the transport current is switched off,

$$\frac{J(x)}{J_c} = \begin{cases} \frac{2}{\pi} \left[ \arctan\left(\sqrt{\frac{w^2-a^2}{a^2-x^2}}\right) - 2 \arctan\left(\sqrt{\frac{w^2-b^2}{b^2-x^2}}\right) \right], & -a < x < a, \\ 1 - \frac{4}{\pi} \arctan\left(\sqrt{\frac{w^2-b^2}{b^2-x^2}}\right), & a < |x| < b \end{cases}, \quad (2)$$

where  $a = w\sqrt{1-(I/I_c)^2}$ ,  $b = w\sqrt{1-(I/2I_c)^2}$ . At  $b < |x| < w$  the current density is equal to  $-J_c$ , see Fig. 4(c).

When a large magnetic field was applied to the strip and subsequently removed, the current density  $J(x) = -J_c$  and  $J(x) = J_c$  in the left and the right half of the strip, respectively. If the strip is subsequently biased with transport current  $I$ , then

$$\frac{J(x)}{J_c} = \begin{cases} \frac{4}{\pi} \arctan\left(\sqrt{\frac{(w/2)^2-a^2}{a^2-(x+w/2)^2}}\right) - 1, & -w/2 - a < x < -w/2 + a, \\ 1, & -w < x \leq -w/2 - a \text{ or } -w/2 + a \leq x < w \end{cases}, \quad (3)$$

see Fig. 5(c). In the remanent state after the current pulse, see Fig. 6(c),

$$\frac{J(x)}{J_c} = \begin{cases} -1 - \frac{4}{\pi} \arctan\left(\sqrt{\frac{w^2-b^2}{b^2-x^2}}\right) + \frac{4}{\pi} \arctan\left(\sqrt{\frac{(w/2)^2-a^2}{a^2-(x+w/2)^2}}\right), & -\frac{w}{2} - a \text{ or } -\frac{w}{2} + a \leq x < b, \\ -1, & b \leq |x| < w \end{cases} \quad (4)$$

\* Email: t.h.johansen@fys.uio.no

<sup>1</sup> C. P. Bean, Phys. Rev. Lett. **8**, 250 (1962).

<sup>2</sup> V. K. Vlasko-Vlasov, M. V. Indenbom, V. I. Nikitenko, A. A. Polyanskii, R. L. Prozorov, I. V. Grakhov, L. A. Delimova, I. A. Liniichuk, A. V. Antonov, and M. Y. Gusev, Superconductivity **5**, 1582 (1992).

<sup>3</sup> M. V. Indenbom, A. Forkl, H. Kronmüller, and H.-U. Habermeier, Journ. of Superconductivity **6**, 173 (1993).

<sup>4</sup> T. H. Schuster, M. R. Koblishka, B. Ludescher, W. Gerhäuser, and H. Kronmüller, phys. stat. sol. (a) **130/2**, 429 (1992).

<sup>5</sup> M. D. Johnston, J. Everett, M. Dhalle, A. D. Caplin, J. C. Moore, S. Fox, C. R. M. Grovenor, G. Grasso, B. Hensel, and R. Flükiger, In: "High-Temperature Superconductors: Synthesis, Processing, and Large-Scale Applications", Ed. by U. Balachandran, P. J. McGinn, and J. S. Abell (TMS, 1966) p. 213.

<sup>6</sup> U. Welp, D. O. Gunter, G. W. Crabtree, J. S. Luo, V. A. Maroni, W. L. Carter, V. K. Vlasko-Vlasov, V. I. Nikitenko, Appl. Phys. Lett. **66**, 1270 (1995).

<sup>7</sup> A. E. Pashitski, A. Polyanskii, A. Gurevich, J. A. Parrell, and D. C. Larbalestier, Appl. Phys. Lett. **67**, 2720 (1995).

<sup>8</sup> M. E. Gaevski, A. V. Bobyl, D. V. Shantsev, Y. M. Galperin, T. H. Johansen, M. Baziljevich, H. Bratsberg, and S. F. Karmanenko, Phys. Rev. B **59**, 9655 (1999).

<sup>9</sup> M. E. Gaevski, D. V. Shantsev, Yu. Galperin, A. V. Bobyl, T. H. Johansen, and H. Hauglin, Phys. Solid State, **41**, 877-880 (1999) [Fiz. Tv. Tela, **41**, 965-968 (1999)].

<sup>10</sup> A. Oota, K. Kawano, T. Fukunaga, Physica C **291**, 188 (1997).

<sup>11</sup> J. Herrmann, N. Savvides, K.-H. Muller, R. Zhao, G. McCaughey, F. Darmann, M. Apperley, Physica C **305**, 114 (1998).

<sup>12</sup> E. Sheriff, D. Giller, Y. Radzyner, A. Shaulov, Y. Schlesinger, Y. Yeshurun, J. Low. Temp. Phys. **117**, 693 (1999).



- <sup>13</sup> S. Shikii, T. Kondo, M. Yamashita, M. Tonouchi, M. Hangyo, M. Tani and K. Sakai, *Appl. Phys. Lett.* **74**, 1317 (1999).
- <sup>14</sup> Y. H. Zhang, Z. H. Wang, H. Luo, X. F. Wu, H. M. Luo, Z. Xu and S. Y. Ding, *J. Phys. Condens. Matter* **13**, 2583 (2001).
- <sup>15</sup> P. Zhang, C. Ren, S. Y. Ding, Q. Ding, F. Y. Lin, Y. H. Zhang, H. Luo and X. X. Yao, *Supercond. Sci. Technol.* **12**, 571 (1999).
- <sup>16</sup> L.P. Ma, H.C. Li, R.L. Wang and L.Li, *Physica C* **291**, 143 (1997).
- <sup>17</sup> Z. Y. Zeng, X. X. Yao, M.J. Qin, Y. Ge, C. Ren, S. Y. Ding, L. P. Ma, H. C. Li, and L. Li, *Physica C* *291*, 229 (1997).
- <sup>18</sup> R. Warthmann, J. Albrecht, H. Kronmüller and Ch. Jooss, *Phys. Rev. B* **62**, 15226 (2000).
- <sup>19</sup> D. Giller, A. Shaulov, T. Tamegai, and Y. Yeshurun, *Phys. Rev. Lett.* **84**, 3698 (2000).
- <sup>20</sup> E. Zeldov, J. R. Clem, M. McElfresh, and M. Darwin, *Phys. Rev. B* **49**, 9802 (1994).
- <sup>21</sup> S. F. Karmanenko, V. Y. Davydov, M. V. Belousov, R. A. Chakalov, G. O. Dzijuba, R. N. Il'in, A. B. Kozyrev, Y. V. Likholetov, K. F. Njakshev, I. T. Serenkov, O. G. Vendic, *Supercond. Sci. Technol.* **6**, 23 (1993).
- <sup>22</sup> L. A. Dorosinskii, M. V. Indenbom, V. I. Nikitenko, Yu. A. Ossip'yan, A. A. Polyanskii, and V. K. Vlasko-Vlasov, *Physica C* **203**, 149 (1992).
- <sup>23</sup> E. H. Brandt, M. Indenbom, *Phys. Rev. B* **48**, 12893 (1993).
- <sup>24</sup> T. H. Johansen, M. Baziljevich, H. Bratsberg, Y. Galperin, P. E. Lindelof, Y. Shen, and P. Vase, *Phys. Rev. B* **54**, 16 264 (1996).
- <sup>25</sup> D.V. Shantsev, A.V. Bobyl, Y.M. Galperin and T.H. Johansen, *Physica C* **341-348**, 1145 (2000).
- <sup>26</sup> Y. Yeshurun, A. P. Malozemoff, and A. Shaulov, *Rev. Mod. Phys.* **68**, 911 (1996).
- <sup>27</sup> A. Gurevich and E. H. Brandt, *Phys. Rev. Lett.* **73**, 178 (1994).
- <sup>28</sup> Th. Schuster, H. Kuhn, and E. H. Brandt *Phys. Rev. B* **51**, 697 (1995).
- <sup>29</sup> M. McElfresh, E. Zeldov, J.R. Clem, M. Darwin, J. Deak, and L. Hou, *Phys. Rev. B* **51**, 9111 (1995).
- <sup>30</sup> M. Darwin, J. Deak, and L. Hou, M. McElfresh, E. Zeldov, J.R. Clem, M. Indenbom, *Phys. Rev. B* **48**, 13192 (1993).